약학석사학위논문

Peptide-functionalized graphene as a tumor-activable theranostic system

펩타이드 수식 그래핀을 이용한 종양조직 활성화 진단/치료 시스템

2017 년 2 월

서울대학교 약학대학원

약학과 물리약학전공

최 선 희

Abstract

Peptide-functionalized graphene as a tumor-activable theranostic system

Sunhee Choi
Physical Pharmacy, Department of Pharmacy
The Graduate School
Seoul National University

Simultaneous cancer therapy and diagnosis, termed ‘theranostics’, have received considerable attention due to requirement of personalized medicine, fulfilling spatiotemporal needs of medication for individual patient. Here, we developed a tumor selectively-activable theranostic system that utilize a conjugate of Cy5.5, polyethylene glycol (PEG), and chimeric peptide which engineered to include a matrix metalloproteinase (MMP)-cleavable sequence, a spacer sequence, and a binding sequence for graphene nanosheet (GN). Cy5.5-PEG-chimeric peptide-modified GN clearly marred the fluorescence of Cy5.5 and cell-penetrating function of therapeutic peptide modified onto GN due to quenching ability of GN, and stealth effect of PEG, respectively. With the presence of MMP, cleavage of chimeric peptide released Cy5.5-PEG from GN, facilitating recovery of fluorescence of Cy5.5 and exposure of cell penetrating peptide on the surface of

GN. Deletion of MMP-cleavable sequence in this theranostic system showed negligible differences in fluorescence and antitumor effect upon exposure to MMP. Intravenous administration of MMP-cleavable PEG-GN into SCC7 tumor-bearing mice resulted in 7.2-fold higher fluorescence intensity at tumor site than that of MMP-non-cleavable PEG-GN after 24 hours. Furthermore, cell-penetrating peptide delivered by MMP-cleavable PEG-GN revealed the highest antitumor effect, showing 80% regression of tumor volume than untreated group. Overall, our results demonstrate that tumor-activable PEG-GN could serve as a nano-theranostic system for tumor selective imaging and therapy.

Keywords : theranostics, graphene nanosheet, tumor microenvironment, matrix metalloproteinase, anticancer effect

Student number : 2015-21903

Contents

List of Figures

1. Introduction

Theranostics as a combination of therapy and molecular imaging has recently emerged as a promising way to satisfy unmet needs toward personalized medicine (Schork, 2015; Ryu et al., 2014; Mura et al., 2012). Theranostic therapy enables physicians to track the drug whether it reached to target site, predict the effect of drug and adjust treatment recipe individually (DeNardo et al., 2012). To obtain successful theranostic results, both imaging probe and drug should properly arrive at target site with sufficient amount. Fortunately, abundant researches in delivering system of therapeutic drugs as well as those carrying diagnostic probes have been made by nanotechnologists. Besides, nanotechnologists stepped into developing theranostic nanosystems using chitosan-based nanoparticles, polymer dendrimers, magnetic nanoparticles and carbon nanomaterial (Lim et al., 2013; Kim et al., 2010; Kojima et al., 2012; Shubayev, 2009; Chen et al., 2015). However, most of them expected tumor imaging through passive or active tumor accumulation of nanosystem carrying imaging probe. If the imaging value changes due to tumor-selective factor, it would be advantageous in diagnostic selectivity.

Overexpressed secretomes in tumor microenvironment are good guide to separate tumor lesion from normal tissue. Matrix metalloproteinases (MMPs), a family of endopeptidases, is known to be largely secreted from cancer cells and stromal cells. Originally, MMPs are involved in various physiological processes including tissue remodeling, organ development and inflammatory reactions (Kessenbrock et al., 2010). At tumor site, MMPs enormously influence tumor

progress by affecting angiogenesis, cancer cell growth, tumor invasion and metastasis. They are not only upregulated but also show increased enzymatic activity in the tumor microenvironment. Thus, peptide substrate which is cleaved selectively by MMP will be useful to find out the location where MMP level is high, probably tumor site (Seltzer et al., 1990; Bremer et al., 2001; Xin et al., 2014).

Graphene oxide (GO), two-dimensional carbon nanosheet synthesized from graphite, has been widely applied to cancer therapy due to several applicable properties such as strong mechanical strength, large surface area, good aqueous dispensability, and remarkable thermal property (Kumar et al. 2015). Graphene derivatives including GO can non-covalently bind chemicals having aromatic rings such as doxorubicin, cholesterol, proteins, and DNA, via π-π stacking or Van der Waals interactions (Dreyer et al., 2010; Lu et al., 2010). Our previous study functionalized the surface of reduced graphene oxide (rGO) using cholesterol as an anchoring moiety and successfully enhanced physical stability of rGO in physiological condition (Miao et al., 2013). Besides, graphene derivatives are good quencher of fluorescence, taking excited electron away from fluorescent dye (Kim et al., 2009). Various forms of graphene based biosensors has been developed to detect several disease-related biomarkers including interferon-γ, thrombin and troponin I (Kim et al., 2014; Lu et al., 2009; Chang et al., 2010; Bhatnagar et al., 2016). These researches imply that graphene nanosheet (GN) is a useful tool for theranostics.

In this study, we designed a non-covalently functionalized GN as a tumor-

activable theranostic system by inserting MMP-sensitive peptide (MSP) between graphene-binding chimeric peptide and PEG, to give tumor-selective dequenching effect by graphene on Cy5.5 that is conjugated to the end of PEG. Cleavage of MSP could cause release of PEG-Cy5.5; this would help Cy5.5 to revive its fluorescence and reveal therapeutic drug on the surface of the graphene. As a model drug, buforin IIb was used.

2. Materials and methods

2.1. Synthesis of peptides (F7D4-PEG-Cy5.5 and F7D4MSP-PEG-Cy5.5, F7-BF-FITC)

Three peptides were synthesized for this study. Buforin IIb, a 21 amino acid peptide derived from buforin of the Asian toad Bufo gargarizans, and a peptide including MMP-cleavable sequence (Zhang et al., 2015; Xin et al., 2014; Seltzer et al., 1990) were linked to seven phenylalanines and four aspartates at N-terminal. The sequences are FFFFFFFDDDD-RAGLQFPVGRLLRRLLRRLLR (T-Bu) and FFFFFFFDDDD-PLGVRGG. A peptide without MMP-cleavable sequence, FFFFFFFDDDD-G, was used as a negative control.

All peptides were synthesized by the solid-phase method (Merrifield, 1963). Briefly, 177 mg of resin is stirred in 3mL of dimethylformamide (DMF) for 1h in order to synthesize 0.2 mmol of peptides. After removal of DMF, 0.5 mmol of O-(Benzotriazol-1-yl)-N,N,N',N'-tetramethyluronium hexafluorophosphate (HBTU), 1-hydroxybenzotriazole (HOBt), N,N-diisopropylethylamine (DIPEA) and the first amino acid from the C-terminal of peptide, here, Fmoc-Gly-OH, solution in 2 mL of DMF is added to the resin and stirred for 24 h. Then, the resin is washed with DMF and dichloromethane (MC) 3-4 times. Fmoc amino-protecting group is cleaved after the resin is stirred in 2 mL of piperidine:DMF = 2:8 solution 3 times, 5 min each time. After washing with DMF and MC 3-4 times again, HBTU, HOBt, DIPEA, and next amino acid is added and stirred for 3 h. The step from washing to addition of amino acid is repeated until the last amino acid

attachment is finished. The crude peptides were stripped from the resin by trifluoroacetic acid and purified by either fractional crystallization by adding cold ethyl ether and dialysis in water for 48 h. These purified peptides were analyzed by MALDI-TOF/TOF 5800 System (AB SCIEX, Foster city, CA, USA) and had correct amino acid.

To attach PEG at the C-terminal of peptides, HBTU, HOBt, DIPEA, synthesized peptide, and Cy5.5-PEG-NH2 are dissolved in DMF at a mole ratio 1:1:3:1:1 and stirred for 24 h. The crude peptide-PEG product is purified by dialysis in water for 48 h.

The final products were FFFFFFFDDDD-PLGVRGG-PEG_{2000}-Cy5.5 and FFFFFFFDDDD-G-PEG_{2000}-Cy5.5.

2.2. Detection of peptide cleavage

To confirm the cleavage of peptide by MMP-2, Fluorescein isothiocyanate (FITC)-conjugated peptide with MMP-cleavable sequence and biotin (biotin-MSP-FITC) was purchased from Peptron Inc. (Daegeon, Korea).

Biotin-MSP-FITC (1 μM) was added to each well of streptavidin-coated plate (Pierce Biotech, Rockford, IL, USA). It was incubated at 4 ^{o}C overnight. The solution was aspirated and washed with wash buffer solution. Wash buffer with or without 500 nM of MMP-2 (Sigma-Aldrich, St. Louis, MO, USA) was added to each well and incubated at room temperature overnight. The supernatant of each well was transferred into 96-well black/clear bottom plate. The fluorescence

intensity at 525 nm was measured using a fluorescence microplate reader (Gemini XS; Molecular Device, Sunnyvale, CA, USA).

Cleavage of peptide loaded on graphene nanosheet was also observed. Cy5.5-pMSP-GN solution was prepared in PBS. MMP-2 was added to make the final concentration 500 μM, and incubated for 1 hour. Then samples were centrifuged at 3000 x g for 10 minutes. The supernatant and the pellet were transferred to well plate. The intensity of fluorescence was measured using an eXplore Optix system (Advanced Research Technologies Inc. Montreal, Canada).

2.3. Preparation of surface functionalized GN

Graphene oxide (GO) was prepared from graphite powder following a modified Hummer's method (Li et al., 2008). Briefly, graphite powder (0.5 g; Sigma-Aldrich) was added to cold H_2SO_4 (23 mL). While this mixture was gradually stirred on ice, $KMnO_4$ (3 g) and $NaNO_3$ (0.5 g) were added slowly. The resulting mixture was further stirred for 1 h at 35 ^oC. Subsequently, 46 mL of triple-distilled water (TDW) was added and the mixture was incubated at 90°C for 1 h. The reaction was halted by adding 140 mL of TDW and 10 mL of 30 % H_2O_2. The reaction product was washed and purified by repeated centrifugation, first with an aqueous 5 % HCl solution and then with TDW (three times). Finally, the product was suspended in TDW and sonicated for 2 h to exfoliate the GO layers into GO nanosheets. Unexfoliated GO was removed by centrifugation at 1600 x g for 10 min. The supernatant containing GO nanosheets was collected and filtered through

0.2-μm polycarbonate membrane filters (Millipore Corp., Billerica, MA, USA) using an extruder (Northern Lipid, British Columbia, Canada). The obtained GO nanosheets dispersed in TDW were stored at 4 ^{o}C until use. The final concentration of the prepared GO was 10 mg/mL.

For surface modification, Cy5.5-PEG chimeric peptides with or without MMP-cleavable sequence (F7D4-PEG-Cy5.5 and F7D4-MSP-PEG-Cy5.5) solution in DMSO (5 mg/mL) were added to GN in TDW (10 mg/mL) at a weight ratio of 5:1, and incubated for 5 min at room temperature to make GN functionalized by Cy5.5-PEG (pGN) and Cy5.5-PEG-MSP (pMSP-GN).

2.4. Characterization

The hydrodynamic diameters and lateral dimensions of nanosheets, with or without chimeric peptide-PEG-Cy5.5, were determined by dynamic light scattering using a He-Ne laser (10 mW). Zeta potential values of nanosheets (diluted in TDW) were determined by laser Doppler microelectrophoresis at an angle of 22° using an ELS-8000 instrument (Photal, Osaka, Japan).

Transmission electron microscopy was conducted using a JEM1010 (JEOL, Japan). 5 μL of sample was dropped on a carbon-coated copper grid and dried at room temperature. The dried specimens were then imaged at the accelerating voltage of 80 kV.

Atomic force microscopy was performed using XE-100 (Park Systems, Suwon, Republic of Korea) to measure thickness of peptide-modified nanosheets.

Silicon wafer were cut into 5 mm x 5 mm sections and washed for 30 min with sonication in ethanol. The sections were silanized for 30 min in a solution of 3-aminopropyltriethoxysilane (Sigma-Aldrich) with TDW (1:9, v/v) and one drop of hydrochloric acid (Sigma-Aldrich), and washed with TDW. Next, the sections were soaked in solutions of samples (10 μg/mL) for 10 min, and rinsed with TDW. Then they were immersed in PEG-peptide conjugation sample solutions (10 μg/mL) for 10 min. Finally, they were baked in a 70 ^{o}C oven for 20 min. All the images were obtained in non-contact mode.

2.5. Dequenching ability test of pMSP-GN

The recovery of fluorescence was examined by incubation time change and concentration of MMP-2. SCC7-tumor-bearing mice were sacrificed and tumor was extracted. The obtained tumor was homogenized with addition of PBS buffer. After centrifugation of the homogenized solution at 3000 x g for 10 minutes, the supernatant was obtained. The concentration of MMP-2 was measured using Total MMP-2 Quantikine ELISA kit (R&D systems, Minneapolis, MN, USA).

pGN and pMSP-GN were prepared in SCC7 tumor supernatant. To adjust the concentration of MMP-2, SCC7 tumor supernatant was diluted with PBS. At time points 0, 2, 4 h, the intensity of fluorescence was assessed using an eXplore Optix system.

2.6. Loading of T-Bu onto nanosheets

To load T-Bu on pMSP or pMSP-GN, T-Bu solution in DMSO (5 mg/mL) and Cy5.5-PEG-chimeric peptides (F7D4-PEG-Cy5.5 or F7D4-MSP-PEG-Cy5.5) were subsequently added to GN. The weight ratio of GN, T-Bu, Cy5.5-PEG-chimeric peptides was 5:1:1.

2.7. Hemolysis assay

Mouse blood (500 μL) were collected directly into a heparinized vacutainer tube, washed three times by mixing with PBS and being centrifuged at 500 x g for 10 min. The mouse red blood cells (RBC) were obtained by suspending the pellet in PBS. The RBC density was 2 x 10^9 cells/mL. Samples were prepared at the T-Bu concentration of 0.05 mM in 5 % glucose aqueous solution. 200 μL of samples were mixed with 800 μL of RBC, incubated at 37.5 ^{o}C for 1 hour and centrifuged at 500 x g for 5 min. Triton X-100 was used as a positive control with 100 % hemolysis. Supernatant from each samples were transferred to 96-well plate and the absorbance was measured at 410 nm.

2.8. In vitro anti-cancer efficacy test

Mouse SCC7 cells were cultured in DMEM medium (Welgene, Daegu, South Korea) supplemented with 10% fetal bovine serum, 100 units/mL penicillin, and 100 μg/mL streptomycin (complete DMEM media). SCC7 cells were seeded onto 48-well plates at a density of 2 × 10^4 cell/well. The following day, cells were treated with pGN/T-Bu or pMSP-GN/T-Bu at T-Bu concentration of 150 μg/mL,

with or without MMP-2 at concentration of 500 nM. After 2 h incubation at 37 ^{o}C, the cells were washed twice with media and the extent of cell viability was quantified using 3-(4,5-dimethylthizol-2-yl)-2,5-diphenyltetrazolium bromide (MTT) assay. Each well was filled with the mixture of media at the concentration of 500 μM, discarded after 1 h incubation and added dimethyl sulfoxide to dissolve the resulting crystals. The absorbance was measured at 570 nm using a microplate reader (Sunrise Basic; TECAM, Männedorf, Switzerland). Cell viability was expressed as a percentage of that measured in control groups.

2.9. In vivo fluorescence imaging study

In vivo experiments were conducted with five-weeks-old female C3H mice (Orient Bio Inc., Seungnam, Republic of Korea; approved animal experimental protocol number SNU-150609-2). SCC7-tumor-bearing animal models were made by injecting 3 x 10^6 SCC7 cells subcutaneously at the dorsal aspect of the right side of each mouse. In vivo imaging experiment was conducted when tumors had grown to 80-100 mm^3 in volume. The dorsal hair was manually trimmed with an electrical razor and any leftover hair on the skin was removed by applying hair removing cream for 5 min. The skin was washed and dried completely. pGN or pMSP-GN was injected intravenously at the GN dose of 10 mg/kg. The image of Cy5.5 distribution was evaluated by using an eXplore Optix system at the various time point after injection.

2.10. In vivo anti-cancer efficacy test

To evaluate therapeutic anti-cancer effect of pMSP/GN, SCC7-bearing mice were established by injecting 3 x 10^6 SCC7 cells subcutaneously to five-weeks-old female C3H mice as described above. Mice were intravenously administered with free T-Bu, pGN, pGN/T-Bu and pMSP-GN/T-Bu three times with two-days interval. Dose of T-Bu and GN was 2 mg/kg and 10 mg/kg respectively. The first injection was conducted when tumors had reached to 80-100 mm^3 in volume. Tumor volume was calculated with the formulation (long diameter) x $(\text{short diameter})^2$ x 0.5.

For hematoxylin and eosin (H&E) staining, tumors were extracted and weighed on day 21 after the inoculation of SCC7 cells, and fixed in 10 % neutral buffered formalin. Fixative tissues were embedded in paraffin blocks and sliced into 4um thick tumor section. Tumor tissue sections were immunostained with an anti-proliferating cell nuclear antigen (PCNA) antibody (Thermo Fisher Scientific, San Jose, CA, USA) and subjected to terminal deoxynucleotidyl transferase dUTP nick-end labeling (TUNEL) assays (Millipore Corporation, Billerica, MA, USA) to determine cell-proliferation status and apoptosis, respectively. The number of proliferating or apopotic cells were counted using Image-Pro Plus Version 6.0 image analysis software (Media Cybernetics, Inc. Rockvile, MD, USA) from the picture by an Eclipse TE2000-S microscope (Nikon, Tokyo, Japan).

3. Results

3.1. Characterization of pMSP-GN nanoplatform

As illustrated in Fig. 1, F7D4-MSP-PEG-Cy5.5 and T-Bu bind to the surface of each side of GN. The morphology of GN (Fig. 3A) did not show considerable difference from pGN (Fig. 3B) and pMSP-GN (Fig. 3C). The lateral size of GN, pGN and pMSP-GN were 133.4 ± 2.2 nm, 136.8 ± 4.3 nm and 126.0 ± 4.7 nm respectively, and did not differ particularly. Coating with peptide-PEG-Cy5.5 conjugation on GN resulted in decrease of zeta potential values. The surface charge of GN, pGN and pMSP-GN were -56.8 ± 1.6 mV, -76.3 ± 0.6 mV and -73.8 ± 2.3 mV each.

The AFM image showed increase in roughness and thickness of nanosheets by binding of F7D4-PEG-Cy5.5 or F7D4-MSP-PEG-Cy5.5 (Fig. 3D-H). The estimated average of pinnacles of pGN and pMSP-GN were near 3 nm whereas that of GN was 0.5 ± 0.1 nm (Fig. 3H).

3.1. Dequenching of fluorescence following cleavage of peptide

Biotin-streptavidin system was constructed to estimate the cleavage of MSP (Fig. 2A). The fluorescence of supernatant at wavelength of 525 nm was higher when MMP-2 was treated (Fig. 2B).

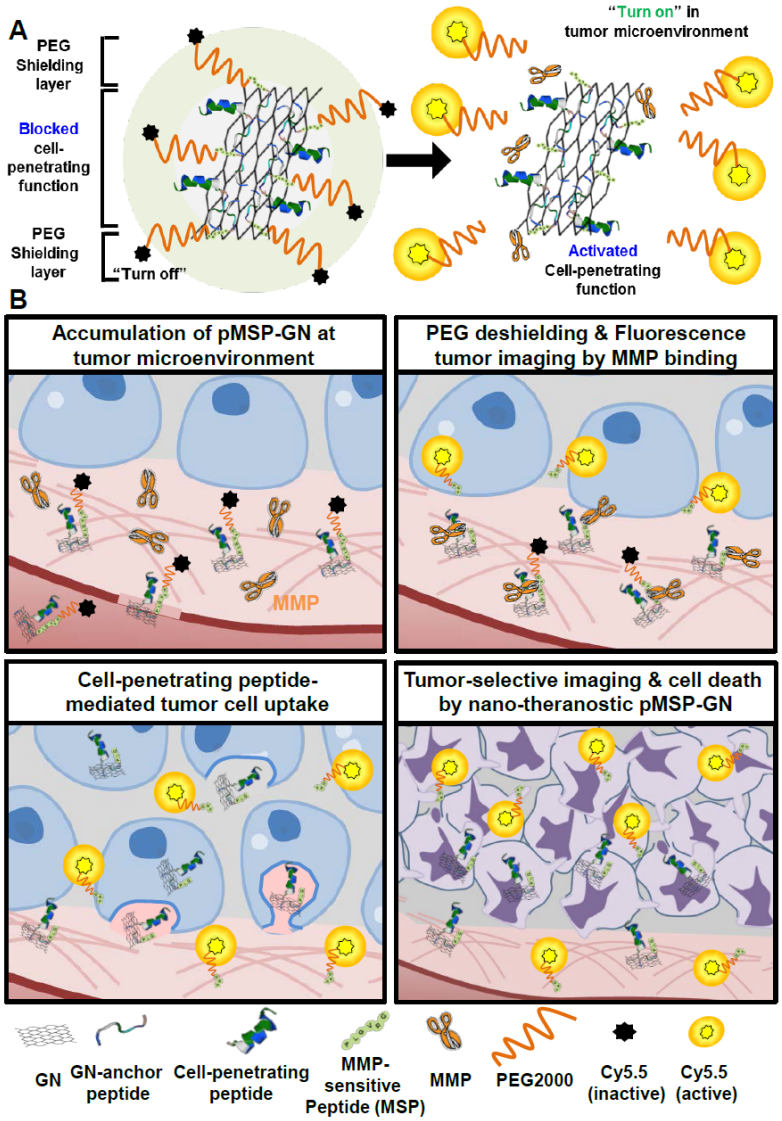

Figure 1. Diagramatic sketch of tumor microenvironment secretome activatable nanoplatform and the hypothesized mechanism of action. (A) The conjugation of Cy5.5, PEG, MSP and anchoring chimeric peptide is bound on GN. Cell-penetrating peptide is loaded on the resulting pMSP-GN and expected to be exposed in the presence of MMP. (B) In the bloodstream, GN and cell-penetrating peptide on it is shielded by PEG. Cy5.5 at the end of PEG is quenched. When nanoplatform reaches near tumor, MMP secreted from tumor cleaves MSP and Cy5.5 is dequenched as Cy5.5-PEG conjugation leaves GN. Cell-penetrating peptide on GN is exposed.

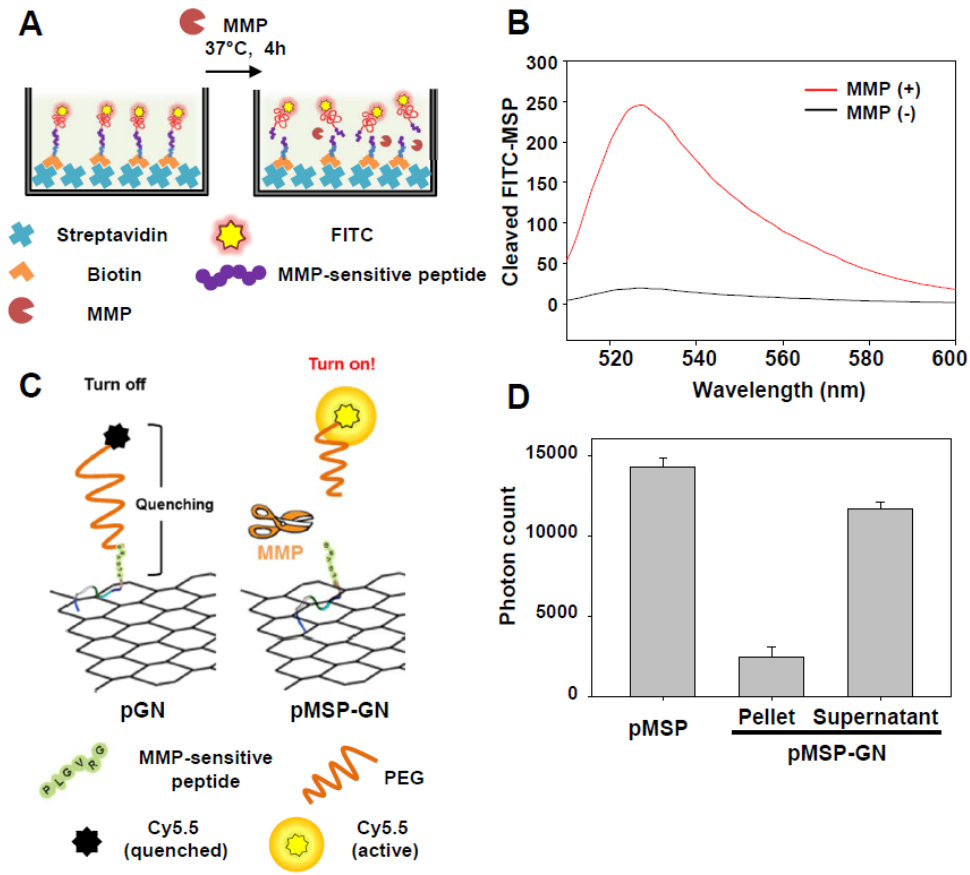

Figure 2. Recovery of fluorescence in the presence of MMP. A diagram of experiment design using biotin-streptavidin interaction (A) and the UV spectrum of the supernatants (B) with or without MMP treatment is shown. Dequenching of Cy5.5 by release of Cy5.5-PEG from GN after MSP cleavage is illustrated (C) and analyzed by fluorometry (D).

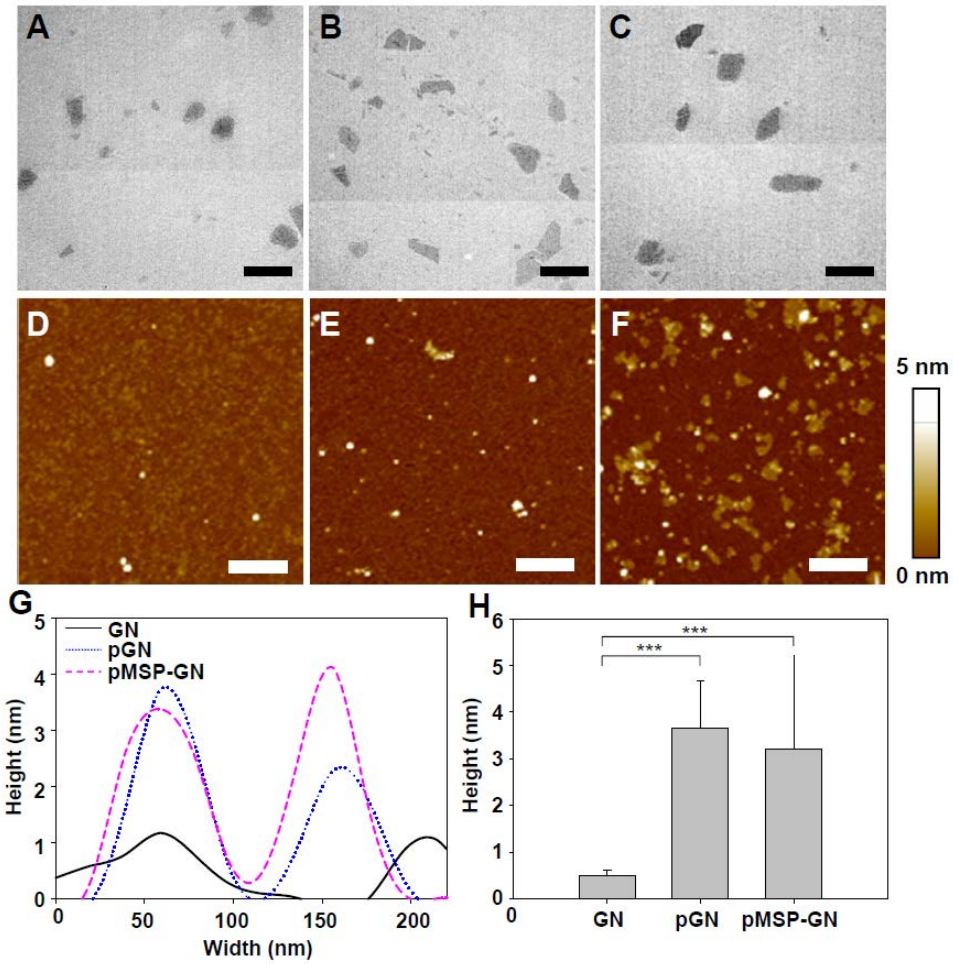

Figure 3. **Characterization of surface-modified nanoplatforms.** TEM images and AFM images of GN (A, D), pGN (B, E), pMSP-GN (C, F) (Scale bar = 200 nm (A, B, C); Scale bar = 500 nm (D, E, F)). Roughness (G) and average thickness (H) of each group was also evaluated (***P< .005).

Instead of biotin, chimeric peptide using seven phenylalanine was used to anchor peptides on GN as shown in Fig. 2C. To confirm the cleavage of MSP and the recovery of fluorescence, pMSP-GN was incubated with MMP-2. The pellet, obtained by centrifugation, showed much lower extent of fluorescence than that of the supernatant (Fig. 2D).

For further tumor-microenvironment mimicking condition, SCC7 tumor secretome was obtained from grated tumor extract. In the presence of SCC7 tumor secretome, pMSP-GN showed higher rate of fluorescence recovery than pGN. Both pGN and pMSP-GN showed tendency of fluorescence increase as incubation time passed (Fig. 4A). After 4 hours incubation with SCC7 secretome, the fluorescence of pMSP-GN increased 5.5-fold while that of pGN increased 1.7-fold. Besides, intensity of fluorescence was proportional to concentration of MMP-2 in SCC7 tumor secretome (Fig. 4B). pMSP-GN also showed more fluorescence rise of 382.6-fold compared with the 24.6-fold rise of pGN.

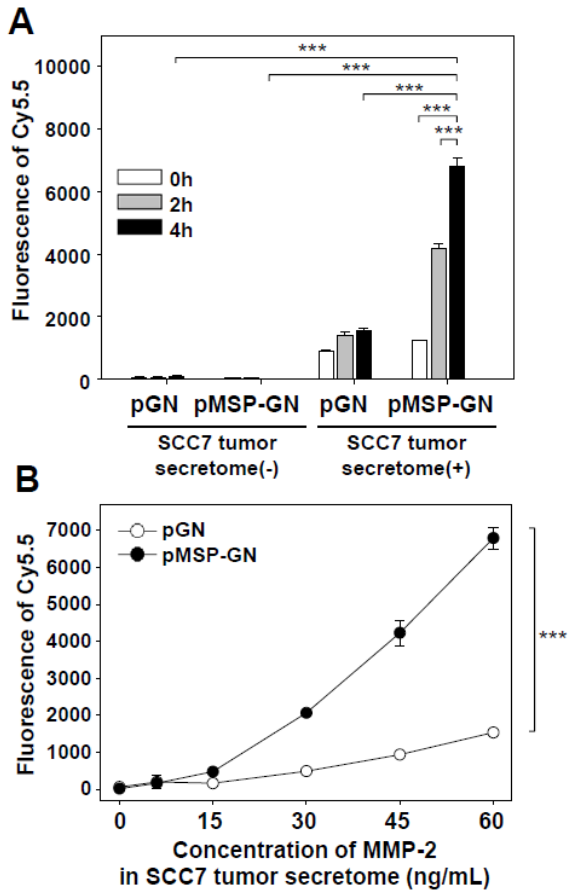

Figure 4. Recovery of fluorescence was observed in time-dependence and concentration-dependence. pGN and pMSP-GN were incubated in SCC7 tumor supernatant for 0, 2, 4 h (A) and in SCC7 tumor supernatant with various concentration for 4 h (B) (n=3; ***P< .005). The samples were centrifuged at 3000 x g for 10 minutes, then the fluorescence of the supernatant were measured using an eXplore Optix system.

3.2. In vitro anti-tumor effect

pMSP-GN/T-Bu nanoplatform was constructed to expose T-Bu when MSP is cleaved out as illustrated in Fig. 5A. The pore-forming ability was figured out in Fig. 5B. T-Bu loaded on GN (GN/T-Bu) revealed 38.4 % of hemolysis ability, a little lower than 52.7 % by free T-Bu. pGN/T-Bu revealed nearly zero (0.03 %) of hemolysis ability even though it was incubated with MMP-2. pMSP-GN/T-Bu showed similar hemolysis ability (34.7 %) with pGN/T-Bu. Consistent with this finding, pMSP-GN showed higher antitumor effect than pGN/T-Bu only when they were treated with MMP-2 (Fig. 5C). Besides, pMSP-GN treated with MMP-2 revealed 2.8-fold higher cytotoxic effect compared to the same pMSP-GN without MMP-2 treatment.

3.3. In vivo imaging by fluorescence distribution of pMSP-GN

Biodistribution of pGN and pMSP-GN was evaluated following *in vivo* administration. Fluorescence recovery and accumulation to tumor site were remarkably different (Fig. 6). From the image of the mice treated with pGN, the intensity of fluorescence at tumor site is negligible. On the other hand, the fluorescence at tumor site of mice treated with pMSP-GN maintained high intensity until 24 h and gradually diminished after then. At 24 h post dose, photon count of pMSP-GN at tumor site was 7.2-fold higher than that of pGN.

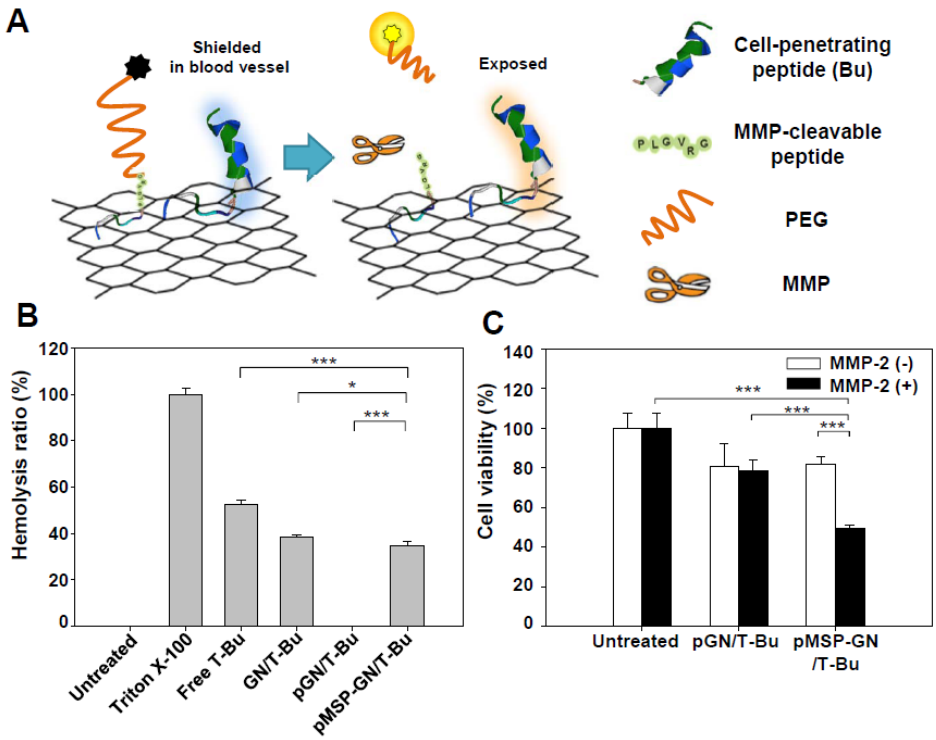

Figure 5. Cytotoxicity of T-Bu loaded on GN. (A) Schematic illustration of process that T-Bu is exposed. (B) Hemolysis assay of T-Bu in free form and loaded form on GN platform was conducted. (C) SCC7 cells were treated with pGN/T-Bu or pMSP-GN/T-Bu for 2 hours. Cell viability was determined by MTT assay (*P< .05; ***P< .005).

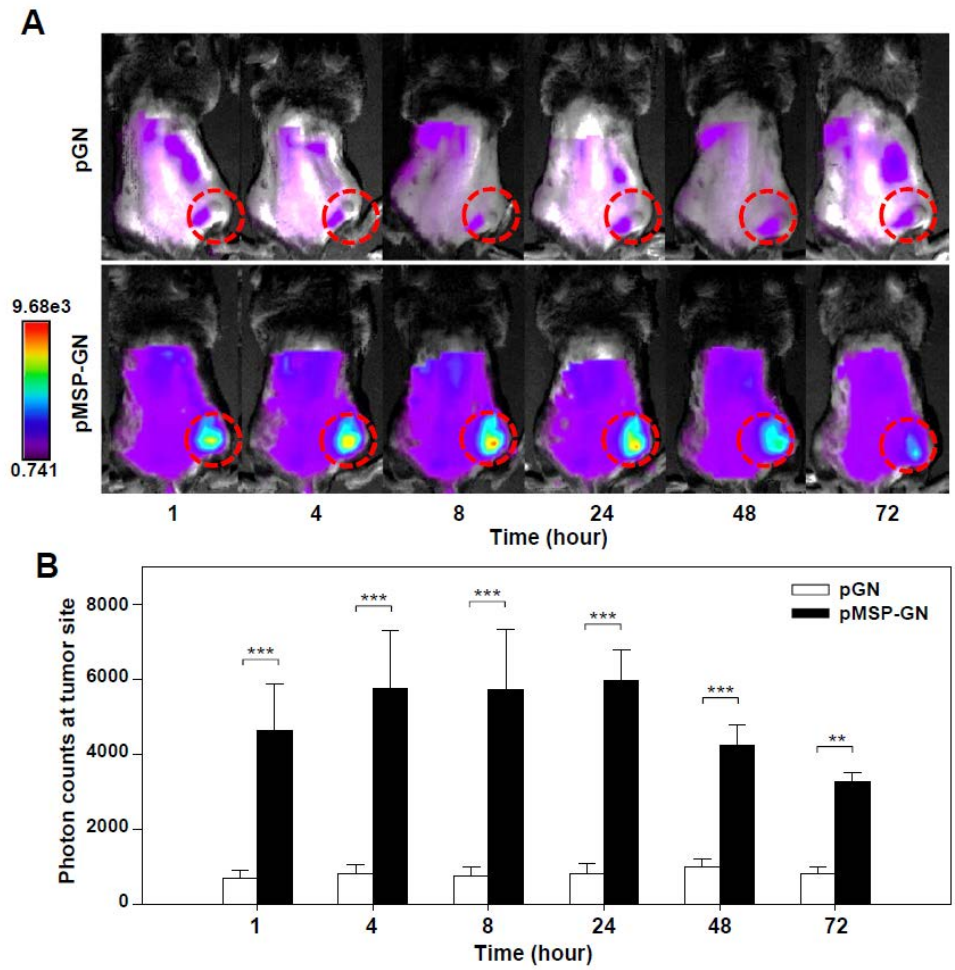

Figure 6. Images of Cy5.5 biodistribution in tumor-bearing mice. SCC7-beaing mice were intravenously treated with T-Bu/pGN or T-Bu/pMSP-GN (2 mg/kg of T-Bu). After 1, 4, 8, 24, 48, and 72 h, the images of biodistribution of Cy5.5 were obtained using an eXplore Optix system (A). The photon counts at tumor site were measured (B) (**P< .01; ***P< .005).

3.4. In vivo anti-tumor effect of T-Bu delivered on pMSP-GN

Delivery of T-Bu via pMSP-GN nanoplatform showed notable antitumor effect to SCC7 tumor-bearing mice. Fig. 7 shows the lowest tumor volume and weight with statistical significance at the group of mice intravenously injected with pMSP-GN/T-Bu as compared to other groups. The tumor volume of the group treated with free T-Bu was larger than those treated with pMSP-GN/T-Bu, and rather similar with pGN or pGN/T-Bu. Prevention of tumor proliferation and apoptosis of tumor cells were also indicated on immunohistochemistry of tumor section on day 21 after inoculation (Fig. 8). The number of proliferating cells, PCNA-positive cells, in the tumor section of pMSP-GN/T-Bu treated mice was 65.2-fold lower than those of untreated mice. Consistently, the number of proliferating cells in the tumor section of pMSP-GN/T-Bu treated group was at least 6.0-fold higher than those of untreated or other groups.

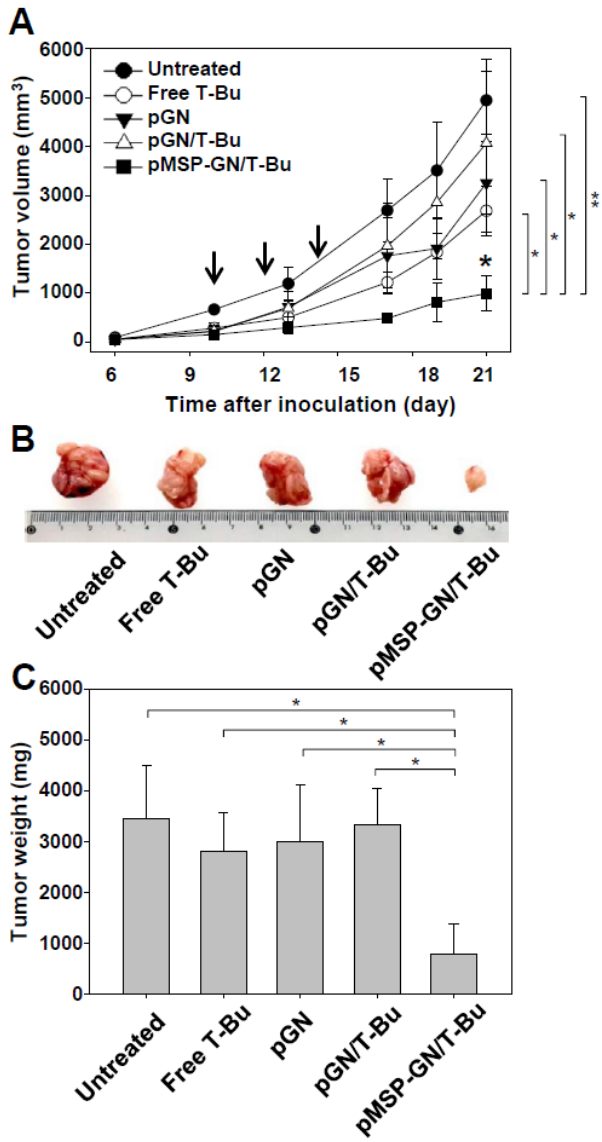

Figure 7. The antitumor effect of T-Bu loaded on nanoplatform. SCC7-bearing mice were treated with free T-Bu, pGN, pGN/T-Bu or pMSP-GN/T-Bu three times with two days intervals. (A) The volume of tumors was measured periodically using calipers until day 21. (B) The picture of tumor which represents tumor size of each group at day 21. (C) The weight of tumors extracted at day 21 was measured (*P< .05; **P< .01).

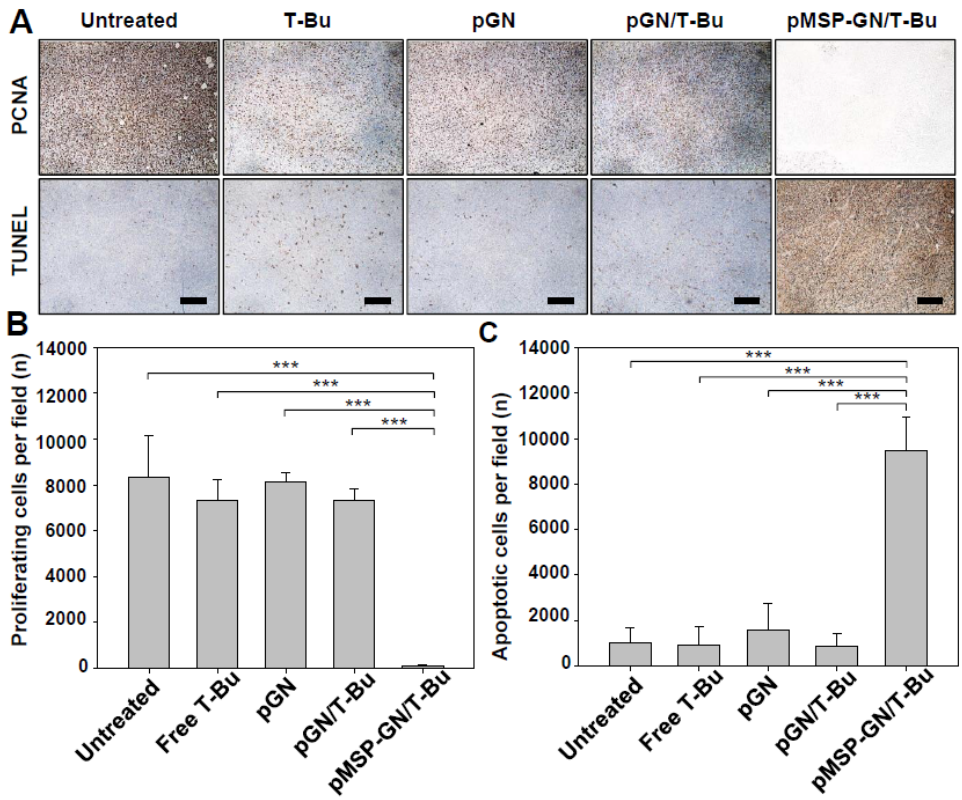

Figure 8. **Immunothistochemistry of tumor tissues.** Tumor tissues were sectioned for anti-PCNA antibody immunostaining (upper line) and TUNEL assay (lower line) (Scale bar = 100 μm). The number of proliferating (B) and apoptotic cells (C) were counted (***P< .005).

4. Discussion

Here, we demonstrated that the system selectively activated near tumor microenvironment could be made using several properties of GN, such as fluorescence quenching ability, ease of surface functionalization and increased biostability under PEG-coated condition. GN based nanosystem that remove PEG tumor-selectively revealed tumor-detecting capability to imaging dye and improved tumor accumulation as compared to pGN and free drug administration, respectively.

Release of dye far from GN was key strategy to activate fluorescence at the therapeutic site. It is widely known that graphite derivatives like GO and reduced GO quench fluorescence of dye due to fluorescence resonance energy transfer or non-radiative dipole-dipole coupling (Loh et al., 2010; Sun et al., 2016). In case of GO, Swathi et al. reported that quenching effect is available when the distance between GO and fluorescent species is less than about 30 nm (Swathi et al., 2009). This unique property has been applied to develop biosensor such as detectors for cardiac marker antigen Troponin I (Bhatnagar et al., 2016), thrombin (Chang et al., 2010), unfolded collagen fragments (Sun et al., 2016). Our results also demonstrate that fluorescence of Cy5.5 was quenched when it was close to GO, and it was recovered when the linker was cleaved out and the freedom of Cy5.5 from GO was given (Fig.2, 4).

T-Bu loaded on GN showed cytotoxic effect only in the presence of MMP-2, when GN is deshielded (Fig. 5). Our result of hemolysis assay (Fig. 5B) implied that F7D4-PEG-Cy5.5 was well anchored, covering the surface of GN so

that they hide pore forming effect of T-Bu. Diverse molecules, as well as short peptide of phenylalanine, with aromatic ring structures were often used as anchoring moiety to modify the surface of GN non-covalently (Kim et al., 2015; Miao et al., 2013). Capability of binding between aromatic species and GN is reported as via π–π interaction. Shim et al. demonstrated that additional seven phenylalanine residue at the N-terminal of buforinIIb enabled its adsorption on rGO with biological activity retained (Shim et al., 2015).

Fluorescence of nanoplatform was also turned on when they were incubated within SCC7 tumor supernatant, depending on incubation time and the concentration of MMP-2 in it (Fig. 4). MMP-2, one of endopeptidases overexpressed in tumor microenvironment, is known to play a role in tumor angiogenesis, growth, and metastasis (Klein et al., 2004). Intensive fluorescence recovery at tumor site of mice which were intravenously injected with pMSP-GN (Fig. 6) reveals that MSP is cleaved out at high level of MMP-2 near tumor site. This result suggests pMSP-GN nanoplatform can be utilized as an indicator for cancer diagnosis.

In addition, the efficacy of tumor regression was the highest at the group treated with pMSP-GN/T-Bu, surpassing the group treated with only T-Bu without any nanocarrier or pGN/T-Bu (Fig.7, 8). Although the distribution of T-Bu was not assessed directly, in vivo efficacy test implies that transmission of T-Bu to incidental place was reduced via our PEG-modified nano-platform as PEG has been broadly applied to drug delivery to achieve long blood circulation of the drug

by preventing nonspecific adsorption to proteins (Hatakeyama et al., 2011). Meanwhile, triggered by MMP-2, T-Bu loaded pMSP-GN nano-platform selectively deliver lager amount of T-Bu to target site as well as indicating where tumor exists.

5. Conclusion

Our results suggest non-covalently functionalized GN for MMP-sensitive anti-tumor therapy and tumor imaging. The introduction of MSP between GN and PEG enabled the tumor-specific increase in fluorescence intensity of Cy5.5 via distance-dependent quenching ability of GN. Loaded with cytotoxic peptide, pMSP-GN exhibited greater antitumor effect compared with free T-Bu, indicating that pMSP-GN would be a useful theranostic system for personalized medicine.

5. References

Bhatnagar D, Kumar V, Kumar A, Kaur I. Graphene quantum dots FRET based sensor for early detection of heart attack in human. *Biosens Bioelectron.* 2016;79:495-9.

Bremer C, Tung CH, Weissleder R. In vivo molecular target assessment of matrix metalloproteinase inhibition. *Nat Med.* 2001;7(6):743-8.

Chang H, Tang L, Wang Y, Jiang J, Li J. Graphene fluorescence resonance energy transfer aptasensor for the thrombin detection. *Anal Chem.* 2010;82(6):2341-6.

Chen D, Dougherty CA, Zhu K, Hong H. Theranostic applications of carbon nanomaterials in cancer: Focus on imaging and cargo delivery. *J Control Release.* 2015;210:230-45.

DeNardo GL and DeNardo SJ. Concepts, consequences, and implications of theranosis. *In: Semin Nucl Med.* 2012;42(3):147-50.

Dreyer DR, Park S, Bielawski CW, Ruoff RS. The chemistry of graphene oxide. *Chem Soc Rev.* 2010;39(1):228-40.

Hatakeyama H, Akita H, Harashima H. A multifunctional envelope type nano device (MEND) for gene delivery to tumours based on the EPR effect: a strategy for overcoming the PEG dilemma. *Adv Drug Deliv Rev.* 2011;63(3):152-60.

Kessenbrock K, Plaks V, Werb Z. Matrix metalloproteinases: regulators of the tumor microenvironment. *Cell.* 2010;141(1): 52-67.

Kim J, Cote LJ, Kim F, Huang J. Visualizing graphene based sheets by fluorescence quenching microscopy. *J Am Chem Soc.* 2010;132(1):260-7.

Kim K, Kim JH, Park H, Kim YS, Park K, Nam H, Lee S, Park JH, Park RW, Kim IS, Choi K, Kim SY, Park K, Kwon IC. Tumor-homing multifunctional nanoparticles for cancer theragnosis: simultaneous diagnosis, drug delivery, and therapeutic monitoring. *J Control Release.* 2010;146(2):219-27.

Kim MG, Park JY, Miao W, Lee J, Oh YK.. Polyaptamer DNA nanothread-anchored, reduced graphene oxide nanosheets for targeted delivery. *Biomaterials.* 2015;48:129-36.

Kim MG, Shon Y, Lee J, Byun Y, Choi BS, Kim YB, Oh YK. Double stranded aptamer-anchored reduced graphene oxide as target-specific nano detector. *Biomaterials.* 2014;35(9):2999-3004.

Klein G, Vellenga E, Fraaije MW, Kamps WA, de Bont ES. The possible role of matrix

metalloproteinase (MMP)-2 and MMP-9 in cancer, e.g. acute leukemia. *Crit Rev Oncol Hematol.* 2004;50(2):87-100.

Kojima C, Cho SH, Higuchi E. Gold nanoparticle-loaded PEGylated dendrimers for theragnosis. *Research on Chemical Intermediates.* 2012;38(6):1279-1289.

Kumar S, Ahlawat W, Kumar R, Dilbaghi N. Graphene, carbon nanotubes, zinc oxide and gold as elite nanomaterials for fabrication of biosensors for healthcare. *Biosens Bioelectron.* 2015;70:498-503.

Li D, Müller MB, Gilje S, Kaner RB, Wallace GG. Processable aqueous dispersions of graphene nanosheets. *Nat Nanotechnol.* 2008;3(2):101-5.

Li X, Deng D, Xue J, Qu L, Achilefu S, Gu Y. Quantum dots based molecular beacons for in vitro and in vivo detection of MMP-2 on tumor. *Biosens Bioelectron.* 2014;61:512-8.

Lim EK, Sajomsang W, Choi Y, Jang E, Lee H, Kang B, Kim E, Haam S, Suh JS, Chung SJ, Huh YM. Chitosan-based intelligent theragnosis nanocomposites enable pH-sensitive drug release with MR-guided imaging for cancer therapy. *Nanoscale Res Lett.* 2013;8(1):467.

Loh KP, Bao Q, Eda G, Chhowalla M. Graphene oxide as a chemically tunable platform for optical applications. *Nat Chem.* 2010;2(12):1015-24.

Lu CH, Li J, Lin MH, Wang YW, Yang HH, Chen X, Chen GN. Amplified Aptamer-Based Assay through Catalytic Recycling of the Analyte. *Angew Chem Int Ed Engl.* 2010;49(45):8454-7.

Lu CH, Yang HH, Zhu CL, Chen X, Chen GN. A graphene platform for sensing biomolecules. *Angew Chem Int Ed Engl.* 2009;48(26):4785-7.

Merrifield RB. Solid phase peptide synthesis. I. The synthesis of a tetrapeptide. *J Am Chem Soc.* 1963, 85(14): 2149-2154.

Miao W, Shim G, Kang CM, Lee S, Choe YS, Choi HG, Oh YK. Cholesteryl hyaluronic acid-coated, reduced graphene oxide nanosheets for anti-cancer drug delivery. *Biomaterials.* 2013;34(37):9638-47.

Mura S and Couvreur P. Nanotheranostics for personalized medicine. *Adv Drug Deliv Rev.* 2012;64(13):1394-416.

Ryu JH, Lee S, Son S, Kim SH, Leary JF, Choi K, Kwon IC. Theranostic nanoparticles for future personalized medicine. *J Control Release.* 2014;190:477-84.

Schork NJ. Personalized medicine: time for one-person trials. *Nature.* 2015;520(7549):609-11.

Seltzer JL, Akers KT, Weingarten H, Grant GA, McCourt DW, Eisen AZ. Cleavage specificity of human skin type IV collagenase (gelatinase). Identification of cleavage sites in type I gelatin, with confirmation using synthetic peptides. *J Biol Chem.* 1990;265(33):20409-13.

Shim G, Lee J, Kim J, Lee HJ, Kim YB, Oh YK. Functionalization of nano-graphenes by chimeric peptide engineering. *RSC Adv.* 2015;5(62):49905-49913.

Shubayev VI, Pisanic TR, Jin S. Magnetic nanoparticles for theragnostics. *Adv Drug Deliv Rev.* 2009;61(6):467-77.

Sun X, Fan J, Zhang Y, Chen H, Zhao Y, Xiao J. A graphene oxide-based FRET sensor for rapid and specific detection of unfolded collagen fragments. *Biosens Bioelectron.* 2016;79:15-21.

Swathi RS and Sebastian KL. Long range resonance energy transfer from a dye molecule to graphene has (distance)− 4 dependence. *J Chem Phys.* 2009;130(8):086101.

Zhang D, Qi GB, Zhao YX, Qiao SL, Yang C, Wang H. In Situ Formation of Nanofibers from Purpurin18-Peptide Conjugates and the Assembly Induced Retention Effect in Tumor Sites. *Adv Mater.* 2015;27(40):6125-30.

국문초록

펩타이드 수식 그래핀을 이용한 종양조직 활성화 진단/치료 시스템

최선희

약학과 물리약학전공

서울대학교

본 연구에서는 항암제 전달 연구를 위한 나노 전달체로서 시아닌 형광 표지인자(Cy5.5), 폴리에틸렌글리콜 (Polyethyleneglycol; PEG)과 펩타이드의 접합체로 표면을 수식한 그래핀 나노시트 (Graphene nanosheet; GN)를 소개하고 있다. PEG와 GN 부착성 펩타이드의 사이에는 종양미세환경에서 많이 발현되는 기질금속단백분해효소 (Matrix metalloproteinase; MMP)에 의하여 잘리는 MMP-sensitive peptide (MSP) 부분을 설계하여 삽입하였다. GN 표면에 펩타이드를 이용한 표면수식은 Cy5.5의 GN에 의한 형광 소거 효과 (Quenching)를 관찰함으로써 확인하였다. SCC7 종양이 형성된 마우스에 정맥 주사한 후 생체 내 조직 분포도를 관찰한 결과, MSP가 없는 펩타이드 접합체로 수식된 GN (pGN)를 주입한 그룹보다 MSP가 있는 펩타이트 접합체로 수식된 GN (pMSP-GN)를 주입한 그룹에서 종양주변 형광 강도가 유의한 수준으로 높았다. 항암 펩타이드로 알려진 부포린IIb (T-Bu)를 탑재하여 주입한 결과, pMSP-GN/T-Bu를 주입한 그룹에서 종양의 크기는 미처리군과 비교했을 때 4.4배 가량 작은 것을 확인하여 높은 항암효과를 나타내었다. 또한, TUNEL assay의 결과로

pMSP-GN/T-Bu를 주입한 그룹에서 세포사멸이 가장 많이 일어난 것을 확인할 수 있었다. 이러한 결과들은 그래핀 나노시트를 이용한 약물전달 시스템이 일반 생체환경에서는 비활성화상태로 유지되다가 종양미세환경에 도달한 후 선택적으로 활성화되고, 약물을 전달하여 세포사멸을 일으켜 항암효과를 일으켰으며, 활성화 시 형광이 되살아남으로써 종양조직 활성화 진단/치료시스템으로써 가능성을 나타낸다.

주요어 : 진단/치료시스템, 그래핀 나노시트, 기질금속단백분해효소, 항암치료제

학번 : 2015-21903